Research Article | Vol. 8, No. 8 | 1 Aug 2017 | BIOMEDICAL OPTICS EXPRESS 3526
Biomedical Optics EXPRESS

Optimizing pulse compressibility in completely all-fibered Ytterbium chirped pulse amplifiers for in vivo two photon laser scanning microscopy

A. Fernández,[1,2,7] L. Grüner-Nielsen,[3] M. Andreana,[2] M. Stadler,[4] S. Kirchberger,[4] C. Sturtzel,[4] M. Distel,[4] L. Zhu,[1,5] W. Kautek,[5] R. Leitgeb,[2] A. Baltuska,[1] K. Jespersen,[6] and A. Verhoef[1,2,8]

[1]*Photonics Institute, TU Wien, Gusshausstrasse 27-29/387, 1040 Vienna, Austria*
[2]*Center for Medical Physics and Biomedical Engineering, Medizinische Universität Wien, Währinger Gürtel 18-20/4L, 1090 Vienna, Austria*
[3]*Danish Optical Fiber Innovation, Åvendingen 22A, 2700 Brønshøj, Denmark*
[4]*St. Anna Kinderkrebsforschung e.V., Children's Cancer Research Institute, Zimmermannplatz 10, 1090 Vienna, Austria*
[5]*Department of Physical Chemistry, Universität Wien, Währinger Strasse 42, 1090 Vienna, Austria*
[6]*NKT Photonics A/S, Blokken 84, 3460 Birkerød, Denmark*
[7]*alma.fernandez@tuwien.ac.at*
[8]*aart.verhoef@meduniwien.ac.at*

Abstract: A simple and completely all-fiber Yb chirped pulse amplifier that uses a dispersion matched fiber stretcher and a spliced-on hollow core photonic bandgap fiber compressor is applied in nonlinear optical microscopy. This stretching-compression approach improves compressibility and helps to maximize the fluorescence signal in two-photon laser scanning microscopy as compared with approaches that use standard single mode fibers as stretcher. We also show that in femtosecond all-fiber systems, compensation of higher order dispersion terms is relevant even for pulses with relatively narrow bandwidths for applications relying on nonlinear optical effects. The completely all-fiber system was applied to image green fluorescent beads, a stained lily-of-the-valley root and rat-tail tendon. We also demonstrated *in vivo* imaging in zebrafish larvae, where we simultaneously measure second harmonic and fluorescence from two-photon excited red-fluorescent protein. Since the pulses are compressed in a fiber, this source is especially suited for upgrading existing laser scanning (confocal) microscopes with multiphoton imaging capabilities in space restricted settings or for incorporation in endoscope-based microscopy.

OCIS codes: (060.2320) Fiber optics amplifiers and oscillators; (320.7090) Ultrafast lasers; (180.4315) Nonlinear microscopy; (180.5810) Scanning microscopy.

References and links

1. W. Denk, J. H. Strickler, and W. W. Webb, "Two-photon laser scanning fluorescence microscopy," Science **248**(4951), 73–76 (1990).
2. K. König, "Multiphoton microscopy in life sciences," J. Microsc. **200**(2), 83–104 (2000).
3. W. R. Zipfel, R. M. Williams, and W. W. Webb, "Nonlinear magic: multiphoton microscopy in the biosciences," Nat. Biotechnol. **21**(11), 1369–1377 (2003).
4. P. J. Campagnola and L. M. Loew, "Second-harmonic imaging microscopy for visualizing biomolecular arrays in cells, tissues and organisms," Nat. Biotechnol. **21**(11), 1356–1360 (2003).
5. F. Helmchen and W. Denk, "Deep tissue two-photon microscopy," Nat. Methods **2**(12), 932–940 (2005).
6. C. Xu and F. W. Wise, "Recent advances in fibre lasers for nonlinear microscopy," Nat. Photonics **7**(11), 875–882 (2013).
7. N. G. Horton, K. Wang, D. Kobat, C. G. Clark, F. W. Wise, C. B. Schaffer, and C. Xu, "In vivo three-photon microscopy of subcortical structures within an intact mouse brain," Nat. Photonics **7**(3), 205–209 (2013).
8. F. W. Wise, "Femtosecond fiber lasers based on dissipative processes for nonlinear microscopy," IEEE J. Sel. Top. Quantum Electron. **18**(4), 1412–1421 (2012).

#294734 https://doi.org/10.1364/BOE.8.003526
Journal © 2017 Received 26 Apr 2017; revised 20 Jun 2017; accepted 22 Jun 2017; published 3 Jul 2017

Biomedical Optics EXPRESS

9. K. Kieu, S. Mehravar, R. Gowda, R. A. Norwood, and N. Peyghambarian, "Label-free multi-photon imaging using a compact femtosecond fiber laser mode-locked by carbon nanotube saturable absorber," Biomed. Opt. Express **4**(10), 2187–2195 (2013).
10. M. Balu, I. Saytashev, J. Hou, M. Dantus, and B. J. Tromberg, "Sub-40 fs, 1060-nm Yb-fiber laser enhances penetration depth in nonlinear optical microscopy of human skin," J. Biomed. Opt. **20**(12), 120501 (2015).
11. E. P. Perillo, J. E. McCracken, D. C. Fernée, J. R. Goldak, F. A. Medina, D. R. Miller, H.-C. Yeh, and A. K. Dunn, "Deep in vivo two-photon microscopy with a low cost custom built mode-locked 1060 nm fiber laser," Biomed. Opt. Express **7**(2), 324–334 (2016).
12. R. Prevedel, A. J. Verhoef, A. J. Pernía-Andrade, S. Weisenburger, B. S. Huang, T. Nöbauer, A. Fernández, J. E. Delcour, P. Golshani, A. Baltuska, and A. Vaziri, "Fast volumetric calcium imaging across multiple cortical layers using sculpted light," Nat. Methods **13**(12), 1021–1028 (2016), doi:10.1038/nmeth.4040.
13. F. Helmchen, M. S. Fee, D. W. Tank, and W. Denk, "A miniature head-mounted two-photon microscope. high-resolution brain imaging in freely moving animals," Neuron **31**(6), 903–912 (2001).
14. W. Göbel, A. Nimmerjahn, and F. Helmchen, "Distortion-free delivery of nanojoule femtosecond pulses from a Ti:sapphire laser through a hollow-core photonic crystal fiber," Opt. Lett. **29**(11), 1285–1287 (2004).
15. C. Xu and W. W. Webb, "Measurement of two-photon excitation cross sections of molecular fluorophores with data from 690 to 1050 nm," J. Opt. Soc. Am. B **13**(3), 481–491 (1996).
16. J. J. Field, R. Carriles, K. E. Sheetz, E. V. Chandler, E. E. Hoover, S. E. Tillo, T. E. Hughes, A. W. Sylvester, D. Kleinfeld, and J. A. Squier, "Optimizing the fluorescent yield in two-photon laser scanning microscopy with dispersion compensation," Opt. Express **18**(13), 13661–13672 (2010).
17. L.-C. Cheng, N. G. Horton, K. Wang, S.-J. Chen, and C. Xu, "Measurements of multiphoton action cross sections for multiphoton microscopy," Biomed. Opt. Express **5**(10), 3427–3433 (2014).
18. S. Tang, J. Liu, T. B. Krasieva, Z. Chen, and B. J. Tromberg, "Developing compact multiphoton systems using femtosecond fiber lasers," J. Biomed. Opt. **14**(3), 030508 (2009).
19. X. Liu, J. Laegsgaard, and D. Turchinovich, "Highly-stable monolithic femtosecond Yb-fiber laser system based on photonic crystal fibers," Opt. Express **18**(15), 15475–15483 (2010).
20. X. Liu, J. Lagsgaard, and D. Turchinovich, "Monolithic highly stable Yb-doped femtosecond fiber lasers for applications in practical biophotonics," IEEE J. Sel. Top. Quantum Electron. **18**(4), 1439–1450 (2012).
21. A. J. Verhoef, K. Jespersen, T. V. Andersen, L. Grüner-Nielsen, T. Flöry, L. Zhu, A. Baltuška, and A. Fernández, "High peak-power monolithic femtosecond ytterbium fiber chirped pulse amplifier with a spliced-on hollow core fiber compressor," Opt. Express **22**(14), 16759–16766 (2014).
22. L. Grüner-Nielsen, D. Jakobsen, K. G. Jespersen, and B. Pálsdóttir, "A stretcher fiber for use in fs chirped pulse Yb amplifiers," Opt. Express **18**(4), 3768–3773 (2010).
23. K. G. Jespersen, D. Jakobsen, P. Kristensen, B. Pálsdóttir, and L. Grüner Nielsen, "Stretcher fibers for chirped pulse amplification at 1030nm and 1550nm," Proc. SPIE **8237**, 82371Q (2012).
24. B. Edvold and L. Grüner-Nielsen, "New technique for reducing splice loss to dispersion compensating fiber," in *proceedings of 22nd European Conference on Optical Communication* (IEEE, 1996) pp. 245–248.
25. J. T. Kristensen, A. Houmann, X. Liu, and D. Turchinovich, "Low-loss polarization-maintaining fusion splicing of single-mode fibers and hollow-core photonic crystal fibers, relevant for monolithic fiber laser pulse compression," Opt. Express **16**(13), 9986–9995 (2008).
26. J. P. Wooler, F. Parmigiani, S. R. Sandoghchi, N. V. Wheeler, D. R. Gray, F. Poletti, M. N. Petrovich, and D. J. Richardson, "Data transmission over 1km HC-PBGF arranged with microstructured fiber spliced to both itself and SMF," in *proceedings of 39th European Conference and Exhibition on Optical Communication* (IEEE, 2013) Tu.3.A.3, DOI: 10.1049/cp.2013.1359
27. M. Distel and R. W. Köster, "In vivo time-lapse imaging of zebrafish embryonic development," CSH Protoc. (2007).
28. M. Distel, M. F. Wullimann, and R. W. Köster, "Optimized Gal4 genetics for permanent gene expression mapping in zebrafish," Proc. Natl. Acad. Sci. U.S.A. **106**(32), 13365–13370 (2009).
29. S. Ramachandran, S. Ghalmi, J. W. Nicholson, M. F. Yan, P. Wisk, E. Monberg, and F. V. Dimarcello, "Anomalous dispersion in a solid, silica-based fiber," Opt. Lett. **31**(17), 2532–2534 (2006).
30. S. H. M. Larsen, M. E. V. Pedersen, L. Grüner-Nielsen, M. F. Yan, E. M. Monberg, P. W. Wisk, and K. Rottwitt, "Polarization-maintaining higher-order mode fiber module with anomalous dispersion at 1 μm," Opt. Lett. **37**(20), 4170–4172 (2012).

1. Introduction

Since its first demonstration in 1990 [1], multiphoton microscopy (MPM) has been established as an indispensable tool for fluorescence imaging in living cells, tissues and living animals with high spatial and temporal resolution [2–4]. The main advantage of nonlinear optical microscopy approaches such as MPM over other imaging approaches is its ability to study cellular processes deeply inside dense tissues and organs in live animals [5]. Efficient multiphoton (MP) excitation requires high peak intensities and therefore typically pulsed excitation sources are required for efficient MP excitation at practical average power levels. Solid state lasers, especially femtosecond Ti:sapphire systems, have dominated the field of

Biomedical Optics EXPRESS

MPM in the spectral wavelength range between 680 and 1300 nm. Despite the remarkable properties and outstanding performance of femtosecond solid state laser sources, there is a fundamental need for easier-to-handle, lower cost and more compact and robust excitation sources to tackle technological barriers towards clinical translation of MPM techniques and for its more widespread use in the world of biological imaging.

Femtosecond fiber lasers are very attractive alternatives to solid state lasers as excitation sources for MPM [6–12]. They can be designed to be environmentally stable, in an all-fiber-integrated architecture, are intrinsically suitable for integration with endoscopic instrumentation and can enable access to new operation parameters that are very challenging to realize with solid state laser sources, such as e.g. higher average power, or high pulse energies at MHz repetition rate. MPM would strongly benefit from the implementation of robust all-integrated fiber based concepts that allow for truly turn-key maintenance-free operation and that at the same time can deliver sufficiently short pulses with high pulse fidelity even to a remote target if required. Flexible fiber-based nonlinear optical endoscopy is of relevance to allow cellular imaging within hollow tissues or solid organs which are typically not accessible to a conventional optical microscope. A fiber delivery concept based on a hollow core fiber offers a flexible means of delivering distortion-free high-peak power pulses on target, which is very attractive for developing instrumentation for high resolution *in vivo* imaging, like multiphoton endoscopes and miniaturized multiphoton microscopes [13,14].

In nonlinear fluorescent microscopy, especially in living tissue, optimizing the MP fluorescent yield is very important for developing highly efficient microscope systems. It has been shown that the time averaged fluorescence photon flux in multiphoton microscopy depends not only on the temporal pulse width but also on the temporal pulse shape at the focus of the excitation source [15–17], therefore appropriate dispersion compensation is relevant to optimize the multiphoton fluorescent yield. In Ref [16]. it was shown that excitation with a transform-limited pulse significantly increases the efficiency of excitation (and thus improves the signal-to-noise ratio of two-photon imaging) as compared to the signal-to-noise ratio obtained using an uncompensated or partially compensated pulse. From the practical point of view, another big advantage of using (close to) Fourier transform-limited pulses for MPM can be seen as follows: since a non-transform-limited pulse of a certain pulse duration has a broader spectrum than a transform-limited pulse of the same duration, the non-transform-limited pulse will broaden faster than the transform-limited pulse when dispersive elements are added or changed in the beam path. This has important practical consequences for the development of compact and simple laser systems for nonlinear optical microscopy because once the system is optimized for highest fluorescence yield, when changing the microscope objective for one with a different design (different dispersion parameters, for example using a higher or lower magnification, or a water immersion objective instead of a ‘dry’ objective) the pulse with the broadest bandwidth (which originally was not transform-limited) will be affected more than the spectrally narrower transform-limited pulse, and the fluorescence yield drop will be more dramatic. Furthermore, in applications such as high speed volumetric calcium imaging, where the goal is to image a big volume in the shortest possible time [12], in order to minimize the rise in tissue temperature, transform limited pulses should be preferred.

When developing highly integrated, high-peak power all-fiber sources delivering high-fidelity pulses for multiphoton microscopy it is important to keep the amount of nonlinearities in the system low and to implement suitable fiber based stretching and compression schemes that will not trade-off pulse duration and pulse fidelity for all-fiber integration. Ideally the pulse duration from such an all-fiber source should be independent of the output pulse energy, to allow a fast change of the excitation power without the use of expensive electro-optic modulators. In standard single mode fibers femtosecond pulses are severely broadened, particularly due to intensity dependent nonlinear effects which start being significant even at

Biomedical Optics EXPRESS

energy levels below 1 nJ. Hollow-core photonic band gap fibers (HC-PBF) are very attractive for the delivery of energetic femtosecond pulses. As most of the optical power is confined in an air-filled core, the amount of nonlinearities experienced by the propagating pulsed are dramatically reduced as compared to pulse propagation through solid core fibers, which makes HC-PBF very attractive for applications in nonlinear optical microscopy, especially *in vivo* nonlinear optical endoscopy.

Previously, a fiber-delivered Yb-femtosecond fiber laser was used for multiphoton imaging [18]. That system uses a piece of HC-PBF to compensate the positively chirped pulses delivered by the amplifier, and delivers 150 fs pulses with 200 mW output at 40 MHz repetition rate. It was noted that the compressed pulses are not transform-limited due to uncompensated residual chirp (higher order dispersion of the fibers). This is expected and similar to other Yb-fiber system realizations using standard single mode fiber (SMF) stretchers combined with HC-PBF compressors, where the highest pulse energy achievable without compromising pulse quality and pulse duration will be limited because of the small stretching ratio imposed by dispersion compensation issues, e.g. the fact that the HC-PBF does not compensate for higher order dispersion terms of the fibers typically used in Yb-fiber amplifiers. In general, there will be a trade-off between the stretching ratio (which determines the achievable pulse energy) and the quality of pulse compression (amount of uncompensated residual chirp) [19–21].

We have previously demonstrated an all-fiber Yb laser operating at a central wavelength of approximately 1060 nm, that uses a 10 μm core large mode area (LMA) Yb-doped fiber as main amplification stage and a dispersion compensating fiber (DCF) [22] stretcher that matches the dispersion of a 25 m long HC-PBF compressor [21] as well as a pigtailed acousto-optical modulator for pulse downcounting. With this configuration, amplification in the linear regime yielded up to 80 nJ, 220 fs pulses at a repetition rate of 2 MHz. This shows that this approach allows achieving higher pulse energies without having to compromise on pulse quality and pulse duration compared to when only standard SMF is used to stretch the pulses.

In this paper, we compare the performance of two different single mode Yb-fiber amplifiers, with a flexible spliced-on HC-PBF compressor operating at the oscillator full repetition rate of 76 MHz for MPM: system I, with a stretcher comprising of SMF in combination with a DCF; and system II, with a simple polarization maintaining (PM) SMF stretcher. With both systems, we have optimized the fluorescent signal from green-fluorescent beads by adjusting the stretcher length and we compare the fluorescent yield (measured fluorescence signal) obtained with the two systems. We further demonstrate the multiphoton imaging capabilities of the system that uses a DCF stretcher by imaging two-photon fluorescence from a stained lily-of-the-valley root, second harmonic generation from *ex vivo* rat-tail tendon, and *in vivo* two-photon fluorescence and second harmonic generation in zebrafish larvae.

2. Experimental setup

2.1 Laser source

A schematic of the laser source is shown in Fig. 1. The seed source is a dispersion managed Yb-fiber oscillator operating at a repetition rate of 76 MHz. A 10-nm full-width at half-maximum (FWHM) portion of the seed spectrum is transmitted through a tunable filter before being amplified in a SMF pre-amplifier. Because of the use of SMF-pigtailed components connecting the oscillator to the pre-amplifier, the pulses at the input of the pre-amplifier are pre-stretched to a duration of approximately 2 ps. A second filter is inserted after the pre-amplifier to suppress amplified spontaneous emission. Before the second amplification stage, the pulses are further stretched to ~30 ps duration in ~10 m of SMF and 4.8 m of DCF [21] (system I) or ~60 m of PM SMF (system II). Design and integration of DCFs is discussed in Refs [22–24]. The seed central wavelength of the amplifier is tuned to be around 1060 nm,

Biomedical Optics EXPRESS

where the (higher-order) dispersion of the compressor is best matched to the accumulated chirp in system I. The final amplifier stage consists of standard PM SMF components and a short length of core-pumped Yb-doped PM fiber (Coractive YB-401P), followed by a low-insertion loss pigtailed Faraday isolator and a ~25 m long HC-PBF (HC-1060-02, NKT Photonics) compressor. The compressor fiber is as flexible as standard SMF and allows for easy handling. Due to the higher NA of the core-pumped Yb-doped fiber compared to the cladding pumped 10-µm core active LMA fiber used in [21], direct angle-splicing of the active fiber to the HC-PBF was not enough for providing sufficient isolation for stable amplifier operation and for suppressing parasitic lasing at all pump powers. The output of the isolator is spliced to the HC-PBF using a Vytran FFS2000 fusion splicer, taking care to achieve a linearly polarized output (as described in detail in [21,25,26]) and to ensure single mode excitation of the fundamental mode. No additional coiling was needed to ensure single mode operation. At the output of the compressor fiber we obtain single-mode linearly polarized pulses with up to 100 mW of average power (~1.3 nJ pulse energy, limited by the available pump power) with an M^2 of <1.2. The output of the compressor fiber is collimated and guided to a fluorescence microscope (Zeiss Axioplan) which we have adapted for laser scanning multiphoton imaging (see Fig. 1). The stretching ratio of the system warrants that the pulse duration at the HC-PBF compressor output is independent of the pump power of the second amplifier stage, and allows further scaling of the output power or pulse energy to several Watts or tens of nJ [21], which can be achieved by replacing the core-pumped second amplifier stage by a cladding-pumped amplifier.

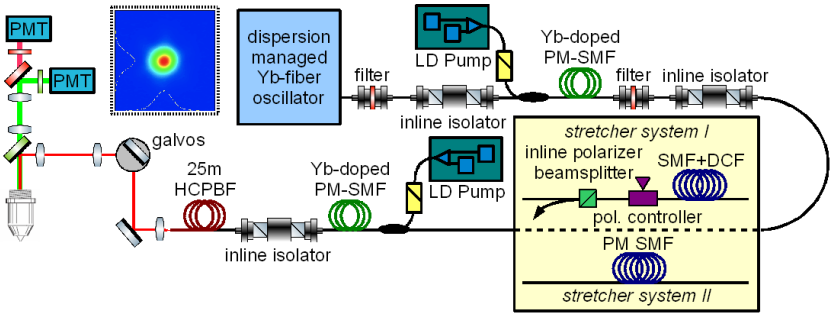

Fig. 1. System layout. The Yb-fiber chirped pulse amplifier is designed to operate with negligible nonlinear phase accumulation, such that the pulse duration at the output of the HC-PBF compressor is independent of the pump power of the second amplifier stage, and thus output pulse energy. The collimated output beam is guided to the laser scanning two-photon microscope (leftmost part of the image). The x-y-position of the focus in the sample plane of the microscope is controlled by two galvanometric mirrors in the beam path. PMT: photomultiplier tube. LD: laser diode. Dashed box inset: measured beam profile with x- and y-projections (full lines) and respective Gaussian fits (dashed lines).

Pulse compression was first optimized for system I by tuning the bandpass filters preceding each of the two amplifier stages together with adapting the length of (passive) SMF, while measuring the output pulse duration using second harmonic frequency resolved optical gating (SH FROG) and maximizing the two-photon excitation induced fluorescence from fluorescent beads. By adapting the length of SMF in the system, the group velocity dispersion of the stretcher is matched to the group velocity dispersion (GVD) of the HC-PBF compressor. Since the amplifier operates in a regime where the accumulated nonlinear phase is negligible, the higher-order phase mismatch can be minimized by tuning the wavelength or changing the ratios between the lengths of DCF, SMF and compressor fiber. Since the DCF stretcher was used as a fixed module with SMF pigtails, and the length of the HC-PBF compressor should also be kept constant, once GVD has been optimized we use wavelength tuning to minimize the third-order dispersion (TOD). The HC-PBF length of 25 m is chosen because the losses in the compressor for that length are roughly 3 dB (50%). A larger

Biomedical Optics EXPRESS

stretching ratio, and consequently longer HC-PBF will therefore not allow to obtain a higher pulse energy at the output. The measured compressed pulses have a duration (258 fs) which is only about 5% longer than the Fourier limited duration (250 fs) corresponding to the spectrum from the laser (see Fig. 2), and ~92% of the energy is contained in the main pulse.

To realize system II, we removed the pigtailed DCF module, and the fiber polarization controller and polarizer directly behind it and replaced them by PM SMF. The optimum length of the PM SMF stretcher was found by measuring the SH FROG trace for best compression and monitoring the fluorescent signal from the green fluorescent beads. The measured compressed pulses for optimum compression are 310 fs long. The maximum output power of system II was 110 mW. No measurable changes in the recorded fluorescent signal are detected for small changes in the stretcher length (± 50 cm) away from optimum. The measured compressed pulses have a duration (310 fs, see Fig. 2) which is about 24 percent longer than the Fourier limited duration (250 fs) corresponding to the spectrum from the laser, and about 70% of the energy is contained in the main pulse.

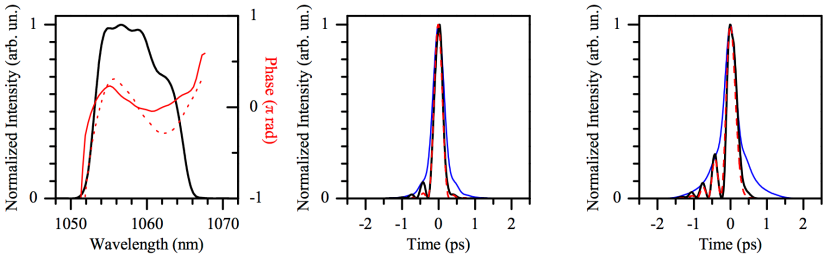

Fig. 2. SH FROG characterization of the compressed pulses from our Yb-fiber CPA. Left panel: laser output spectrum, together with the reconstructed spectral phase of system I (solid red curve) and system II (dotted red curve). Center panel: reconstructed temporal intensity profile (black) and intensity autocorrelation (blue) of system I. The measured pulse duration is 258 fs FWHM, and corresponds well to the expected pulse duration taking into account the amplified spectrum and residual (uncompensated) higher-order chirp calculated for system I (red). Right panel: reconstructed temporal intensity (black) and intensity autocorrelation (blue) of system II. The measured pulse duration is 310 fs FWHM, corresponding well to the expected pulse duration taking into account the amplified spectrum and residual (uncompensated) higher-order chirp calculated for system II (red).

2.2 Multiphoton laser scanning microscope

The two all-fiber Yb chirped pulsed amplifiers described in the previous sections were used as master sources for a laser scanning multiphoton fluorescence microscope (see Fig. 1). A Leica PlanFluotar 40x objective with a numeric aperture (NA) of 0.7, specified to optimally perform with 0.17 mm thin cover glass slips was used for all images. By varying the pump power delivered to the second amplification stage, the laser power at the sample can be varied from ~2 mW up to ~55 mW. Backwards propagating fluorescence (or second harmonic) light is detected in two different color channels using two photon-multiplier tubes (PMT). The light incident on the PMTs is separated from the excitation path using a dichroic beamsplitter (highly reflective in the wavelength range from 1010 to 1080 nm, with high transmission of visible wavelengths), and light detected in the green and red channels is split using a second dichroic beamsplitter (long-pass filter with 590 nm cut-off wavelength). Right in front of each PMT a bandpass filter is inserted (‘red’ 645/75, ‘green’ 535/50 – central wavelength/width, nm) It is important to note that the combination of the excitation wavelength (~1060 nm) and the detection bandwidth in the green channel is such that it is not very well suited for detection of two-photon excitation induced fluorescence. This is easily explained since fluorescence at wavelengths shorter than 530 nm cannot be induced by 1060-nm pulses through two-photon excitation, just because of energy conservation. Considering typical absorption and emission spectra of natural fluorophores, two-photon excitation using 1060 nm wavelength pulses can induce fluorescence at wavelengths longer than 540 nm, and the

Biomedical Optics EXPRESS

bandpass filter in the green channel only transmits light at wavelengths between 510 and 560 nm. However, our green channel is optimally suitable for the detection of second harmonic light generated in the sample.

Using the 0.7 NA objective in combination with the pulses from our fiber laser with the beam overfilling the back-aperture we estimate a spatial resolution of 0.6 µm. Thus, when imaging with our system, the pixel size should not be larger than about 0.6 µm. The imaging system allows scanning a 300x300 μm^2 field-of-view (FOV). For this FOV, raster scanning with our galvanometric scanners can be achieved at a speed of 5 ms per line including 950 µs flyback time. Faster scanning leads to imaging artifacts, due to nonlinear behavior of the galvanometric mirror used for the fast scan axis. Considering the resolution of 0.6 µm, each 300x300 μm^2 frame should consist of at least 500x500 $pixels^2$, which can be acquired at a frame rate of 0.4 Hz with a pixel dwell time of 8 µs.

3. System imaging performance

3.1 Comparing imaging capabilities

In order to compare the imaging performance of the two all-fiber chirped pulsed amplifiers presented here, we have imaged fluorescent beads (Dragon Green fluorescent polymer, mean ∅ 15.45 µm, Bangs Laboratories Inc) and determined the total fluorescence signal achieved with each system after being optimized for best compression as described in section 2.1. After having optimized the dispersion of both systems, we imaged 25 frames of a fixed 300x300 μm^2 area of a sample of the green fluorescent beads fixed between a microscope slide and 0.17 mm thin cover slip at a series of 9 different output powers from both systems, first with system II, and then with system I. Since the fluorescence yield with system II is expected to be lowest, measuring with system II first reduces possible artefacts due to photo-darkening. To illustrate that the same FOV was imaged for all 450 frames, the left panel of Fig. 3 shows a composite image where the red channel corresponds to the average of 25 frames taken with system II at 0.17 nJ pulse energy (~13 mW) on the sample, the green channel corresponds to the average of 25 frames taken with system II at 0.6 nJ pulse energy (~45 mW) on the sample, and the blue channel corresponds to the average of the last 25 frames taken with system I (at 0.6 nJ pulse energy on the sample). The image appears greyscale because the images used for the three color channels exactly overlap, which proves that the same FOV was imaged for all 450 frames. The average signal in the FOV for each image of the series was computed and the results are plotted in the right panel of Fig. 3. Both the signal vs. pulse energy curve for system I and system II are fitted to a power-law ($y = a\,x^b$). For both curves the fitted value for b is 1.97, indicating we observed no saturation of the fluorescence nor significant photodarkening. For the same pulse energy, the signal obtained when using system I was always ~80% higher than the signal obtained when using system II.

It is worth noting that even at these relative long pulse durations (>200 fs), higher order dispersion compensation plays a significant role for maximizing the fluorescence yield. The main reason for this is that in all-fiber systems consisting of several (tens of) meters of fiber the amount of dispersion is quite considerable (GDD and TOD of 1 m of SMF are ~20,000 fs^2 and ~60,000 fs^3 respectively, and GDD and TOD of 1 m of HC-PBF are ~– 60,000 fs^2 and ~400,000 fs^3; note that while the sign of GDD introduced by the HC-PBF is negative, SMF and HC-PBF both introduce positive TOD) as compared to the amount of dispersion introduced by the microscope system and other optical elements in the optical imaging path (typically ~1,000 fs^2 and ~3,000 fs^3 respectively). In contrast, for typical microscope systems seeded by free space solid state lasers that provide near Fourier transform-limited pulses at their output the effect of higher order dispersion compensation (for optimizing the fluorescence signal) starts to be more relevant at much shorter pulse durations (approximately 50 fs) as reported in [16].

Biomedical Optics EXPRESS

Imaging the fluorescent beads also serves to calibrate the FOV of our system. The beads have a diameter of 15.45 µm, and the steep edges of the beads in the image indicate that our setup focuses to a diffraction-limited spot size of ~1 µm diameter. A scan angle of ± 2.5 degrees of the galvanometric mirrors corresponds to a FOV of 300x300 µm^2. Smaller scan angles lead to a proportionally smaller FOV. As noted before, green fluorescence is only very inefficiently excited and detected in our setup, but the ability to detect fluorescence (which is detected clearly in the green detection channel, and only very weakly in the red detection channel) from the Dragon Green beads demonstrates also that one can detect and distinguish fluorescence from different fluorophores, i.e. with our source one can excite green (or yellow) and red fluorescent fluorophores at the same time through two-photon excitation, and distinguish them with high contrast. Because of the superior performance of system I, we used system I for all further measurements.

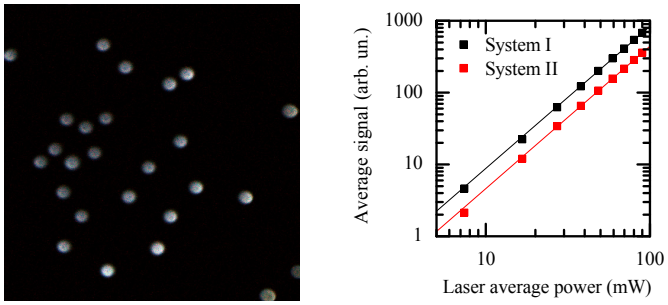

Fig. 3. Left: a 300x300 µm^2 image (500x500 pixels) of Dragon Green fluorescent beads (15.4 µm diameter) between a microscope slide and 0.17 mm thin coverslip. The image is a composite of three images that are the result of averaging 25 frames at low laser power with system II (red image channel), full laser power with system II (green image channel) and full laser power with system I (blue image channel). The size of the beads is used to calibrate the field-of-view of the microscope, and the steep edges of the beads in the image indicate a diffraction limited ~1 µm diameter of the excitation volume at the focus of the microscope, and a ~0.6 µm spatial resolution of our imaging system. Brightness and contrast of the three color-channels of the image are adjusted manually for good visibility of all beads. The excellent overlap of all three color-channels illustrates that no sample movement occurred during the 18 measurements at different laser powers with the two systems. Right: average fluorescence signal versus laser power for the two different laser systems: System I, using SMF and DCF stretcher, black symbols (measurement) and line (fit); System II, using only PM-SMF stretcher, red symbols (measurement) and line (fit).

3.2 Stained lily-of-the-valley root

Lily-of-the-valley (*Convallaria majalis*) root is known for its distinct structure and fine details, and staining with different dyes yields strong fluorescence in various colors from distinct features. Because of these features fixed samples of the lily-of-the-valley root are widely used as test or training samples for fluorescence and confocal microscopy. The same features make such a sample ideal to demonstrate the imaging capabilities of our system. Figure 4 shows an image that is composed of six 300x300 µm^2 (500x500 pixel) frames, each shifted from the other (in the x and/or y direction) by 150–200 µm. Each frame consists only of a single acquisition, obtained in 2.5 s. The laser power delivered to the sample was about 20 mW. The individual frames have been slightly cropped in the region of overlap, to reduce visual artifacts such as the pincushion effect caused by the 1 cm separation between the x- and y-galvanometric mirrors and relatively large scan angles. Strong red fluorescence is observed from the cell-wall regions throughout the image, that are stained with fast green dye. Additionally, a weak signal is also observed in the green channel from several distinct, lignin-rich, regions in the root that are visualized with safranin. Safranin has its peak (1-photon) excitation wavelength at 530 nm, and a broad emission spectrum ranging from 545 to 670 nm

Biomedical Optics EXPRESS

with its peak at about 590 nm. This explains that fluorescence from lignin-rich regions is observed in both the green and red channels.

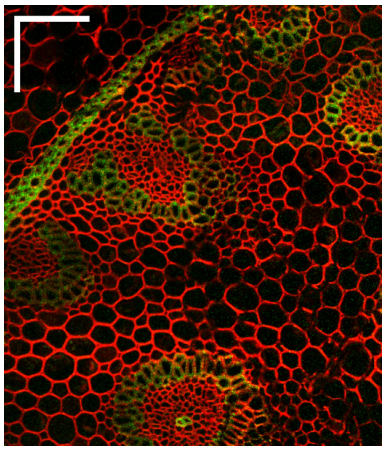

Fig. 4. Image of a fixed stained lily-of-the-valley root. The scale bars correspond to 100 µm. Manual adjustment of the brightness and contrast of the green and red channels in the image make the lignin rich region stained with safranin appear mainly green, although the signal due to fluorescence of safranin is observed in both channels.

3.3 Second harmonic imaging of rat-tail tendon

Rat-tail tendon consists of long aligned strands of collagen fibers. The non-centrosymmetric nature of these fibers causes a large nonzero second order susceptibility, which in a strong enough light field gives rise to second harmonic generation. The dense structure of the tendon makes for strong scattering of the generated second harmonic radiation, which aids efficient detection in the back-propagating direction. We have imaged the second harmonic radiation generated from a rat-tail tendon placed between a microscope slide and 0.17 mm thick cover slip, as show in Fig. 5. Individual strands of collagen fiber can be easily recognized in the 300x300 µm^2 image (500x500 pixels), and the sharp contrast at the edge of the tendon highlights the sub-micrometer resolution obtained with our system.

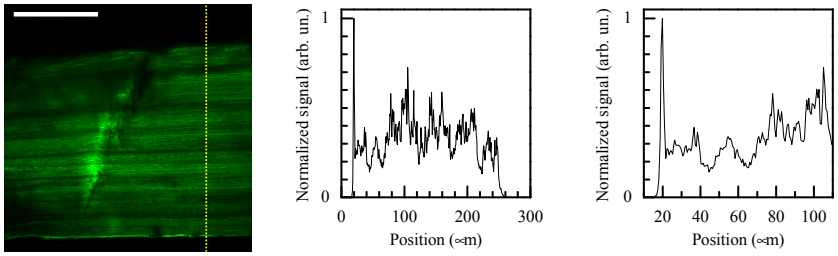

Fig. 5. Left panel: image of a rat-tail tendon mounted between a microscope slide and 0.17 mm thick cover slip. The scale bar corresponds to 100 µm. The steep edges of the tendon and individual collagen fiber strands in the image illustrate the diffraction limited <1 µm resolution of our imaging system. A single 500x500 pixel frame was acquired in 2.5 s, and to improve the image quality (the 5 times higher signal-to-noise ratio allows resolving individual collagen strands even in regions with low signal with good fidelity) 25 frames are averaged. Center panel: cross-section through the image at the location indicated by the yellow dotted line in the left panel. Right panel: zoomed in portion of the center panel.

3.4 In vivo imaging of zebrafish larvae

Finally, we demonstrate the applicability of our all-fibered laser source with DCF stretcher and spliced-on HC-PBF-compressor for *in vivo* multiphoton imaging in relevant biological samples. For this we imaged zebrafish larvae *in vivo*. Transgenic *Et(sp8b:KalTA4GI-*

Biomedical Optics EXPRESS

UAS:mcherry) zebrafish larvae, which show expression of mCherry in the central nervous system, the notochord and in some skin cells, were anesthetized and mounted in low melting agarose onto a 0.17 mm thin cover class in a petri dish as described previously [27, 28].

Figure 6 shows the detected red fluorescence throughout the entire length of a 5 days old larva. The image is composed of 20 frames of 500x500 pixels covering 300x300 µm^2, each shifted in the x and/or y direction from the previous frame. The brightness and contrast are manually adjusted (for each frame equally). For the upper left image, the brightness is set such that only the brightest pixels are slightly saturated, such that fluorescence from the mCherry labeled cells in the central nervous system (blue arrows) is visible. The brightness is increased for the lower left image such that the weak fluorescence from the notochord cell walls (red arrows) is just visible. The upper and lower right images show a zoom of the dashed boxes indicated in the respective left images. Each frame was acquired in 2.5 s.

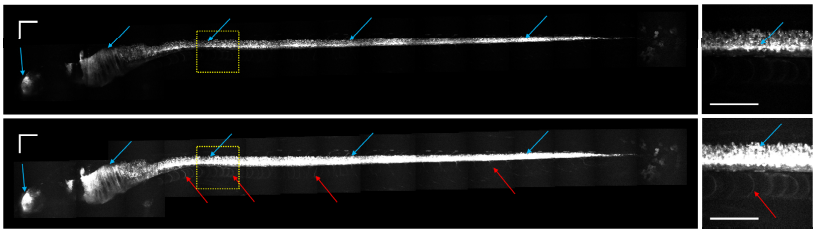

Fig. 6. Two-photon mCherry (red) fluorescence from a 5 days old zebrafish larva. The left images are composed of 20 frames of 300x300 µm^2 each. The scale bars correspond to 100 µm. The upper left image shows the red fluorescence from mCherry-labelled cells, with the contrast set such that only the brightest cells (central nervous system cells, blue arrows) are slightly saturated. The lower left image has the brightness setting increased, such that finer structures with weaker fluorescence, for example from the cell walls of the notochord (red arrows), just below the bright spinal cord, can be seen. The upper and lower right images show a zoom of the dashed boxes indicated in the respective left images.

At an age of around 2 days post fertilization or older, collagen fibers, found for example in the tail fin and muscles of the zebrafish can be detected by imaging the second harmonic light generated from the collagen fibrils. The left part of Fig. 7 shows a 300x300 µm^2 image of the tail of a 5 days old zebrafish larva, with the fluorescence from mCherry labeled skin-cells in the tail fin and nerve cells in the spinal cord (red), and second harmonic generated from collagen fibers in the tail fin (green). A bright green spot is visible from a pigmented cell with stronger scattering. The right part of Fig. 7 shows a 300x300 µm^2 image of a central part along the body of a 2 days old zebrafish larva with second harmonic generated from collagen fibrils in the muscle (green), and fluorescence from mCherry labeled axons (red).

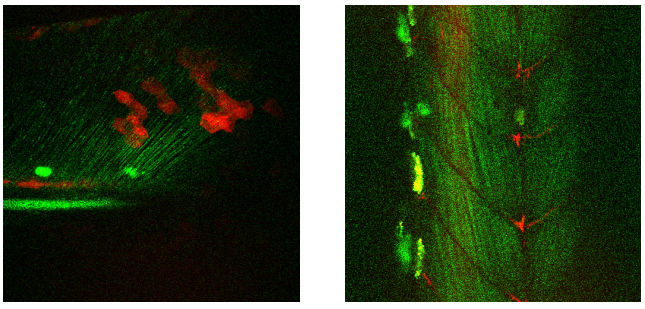

Fig. 7. Image of a 5 days old zebrafish larva's tail (left) and 2 days old larva's muscle tissue (right). The FOV of both images is 300x300 µm^2, the images are composed of 100 and 77 frames respectively. The green line structures are resulting from second harmonic radiation generated from collagen fibrils. The red structures are due to two-photon fluorescence from mCherry labelled cells. The (large) bright green/yellow structures visible are pigmented cells with stronger scattering.

Biomedical Optics EXPRESS

4. Conclusions

We have implemented two simple single mode all-fiber Yb doped amplifiers with spliced-on HC-PBF compressor in laser scanning two-photon microscopy. We have optimized both systems for best pulse compressibility and maximum fluorescence yield. The two systems differ only in the stretcher approach used, which was either a hybrid stretcher consisting of SMF and DCF or a stretcher consisting of only PM SMF. The fluorescent signal from green fluorescent beads obtained with the system using a hybrid SMF/DCF stretcher was 80% higher than for the system with an only PM SMF stretcher. This result shows that in all-fiber Yb laser systems consisting of several (tens of) meters of fiber, phase correction beyond second order dispersion has a strong impact in pulse compressibility and consequently on the two-photon excitation efficiency of the targeted fluorophore even for pulses as long as 250 fs. Therefore, adequate compression schemes that can compensate for higher order dispersion terms need to be implemented for maximizing the signal yield. The dispersion matched strategy implemented through the DCF stretcher – HC-PBF compressor approach used in this work allows for building compact and robust all-fiber integrated systems delivering high quality near transform limited pulses on target. The HC-PBF is very flexible, allows for single mode pulse propagation and good polarization extinction ratio, and it allows for pulse delivery on target with minimized intensity dependent pulse distortions. We expect this approach to prove itself very useful for developing key instrumentation for *in vivo* nonlinear multiphoton endoscopy. In addition, our system offers flexibility when upgrading laser scanning microscope systems with multiphoton capabilities in labs that are not equipped with a big optical bench. Furthermore, the robustness of an all-fiber design facilitates turn-key, maintenance-free operation. The pulses from our laser are compressed to almost Fourier transform limited duration, with very little secondary structure which aids to reduce detrimental effects such as sample heating, and to optimize the multiphoton fluorescent yield. The presented system delivers low energy but the stretching ratio and dispersion-matched stretcher-compressor approach allows to increase the output pulse energy to ~100 nJ by increasing the pump power delivered to the final amplifier stage without compromising the pulse duration and pulse fidelity. Compared to other Yb-fiber systems delivering much higher pulses energies and/or shorter pulses and featuring free space-compressors, our stable all-fiber integrated source offers a more robust design compatible with the development of all-fiber sources with integrated fiber based platforms for flexible multiphoton endoscopes. Since the system operates at 1060 nm, due to the reduced scattering it allows for deeper penetration into tissue than what is typically possible with Ti:Sapphire lasers emitting between 700 and 900 nm. As a proof-of-concept, we have imaged fluorescent beads, a multi-color-stained lily of the valley root as well as second harmonic from rat-tail tendon *ex vivo* and second harmonic and mCherry-fluorescence from zebrafish larvae *in vivo*.

In this system, we were limited by the spectral bandwidth imposed by the two bandpass filters we used for wavelength tuning and ASE suppression. In previous realizations, we have demonstrated shorter pulses (approximately 220 fs). Dispersion compensation becomes more challenging as the bandwidth increases for the DCF stretcher scheme presented here. Nonetheless, it will be possible to compress larger bandwidths to almost Fourier limited durations (yielding shorter pulses), e.g. by using higher-order-mode fibers [29,30] in addition to the DCF, giving additional degrees of freedom to compensate higher order dispersion terms. Also, DCF and HC-PBF can be designed and produced with matching dispersion curves over a broader bandwidth or to target a different central wavelength.

Funding

Austrian Science Fund (FWF) (P23887-N16, T420-N16), European Union (FP7-ICT-317744)

Biomedical Optics EXPRESS

Acknowledgment

We thank T.V. Andersen (NKT Photonics A/S) for his help and advices on splicing and handling the HC-PBF stretcher, NKT Photonics for providing the HC-PBF, and OFS Denmark for providing the DCF stretcher module and measurements of the dispersion of the (PM)-SMF, DCF and HC-PBF.

Disclosures

LG-N: OFS Denmark (E); KGJ: NKT Photonics A/S (E); The authors declare that there are no conflicts of interest related to this article.